Predicting Residual Tensile Strength of Seven-Wire Strands Using That of Single Wires Exposed to Chloride Environments

Radhakrishna G. Pillai[1]; Kenneth F. Reinschmidt, P.E., M.ASCE[2]; David Trejo, P.E., M.ASCE[3]; Paolo Gardoni, M.ASCE[4]; and Mary Beth D. Hueste, P.E., M.ASCE[5]

Abstract: The steel strands in posttensioned (PT) concrete systems are typically embedded inside cementitious grout for protection from the environment. However, strands not embedded in grout have been observed in PT systems. The exposed strand is susceptible to corrosion, and particularly the location where the strand protrudes from the grout (i.e., grout-air-steel interface) is more vulnerable to corrosion. Prediction of the tension capacity (C_T) of strands with such interfaces under various exposure conditions is necessary for structural assessment. This prediction could be accomplished by using the data from an experimental program that includes the exposure of strands to various corrosive environments and testing to determine the time-variant residual C_T of these strands. However, these tests are cumbersome and expensive, especially when it is necessary to maintain very high tensile stress conditions during the exposure period to simulate the in-service stress conditions on the strands in PT systems. Similar investigations of unstressed single wires are simpler and less expensive. This paper presents an experimental investigation of the corrosion-induced losses in the C_T of unstressed wires, unstressed strands, and stressed strands. Based on these data, this paper develops probabilistic models to predict the C_T of unstressed wires with grout-air-steel interfaces and subjected to various moisture and chloride conditions. By using these models for wires and the experimental data on strands, two probabilistic models are then developed to predict the C_T of stressed strands based on the C_T of unstressed wires. The developed models can be used to determine the C_T of strands with grout-air-steel interfaces subjected to various exposure conditions, provided the C_T of corresponding wires under those conditions is estimated. **DOI: 10.1061/(ASCE)MT.1943-5533.0000933.**

Author keywords: Probability; Tensile strength; Corrosion; Prestressing; Posttensioning; Wires and strands; Chlorides; Stress; Voids.

Introduction

High strength, seven-wire, low-relaxation, prestressing strands meeting the ASTM standard A416 (2006) are widely used in posttensioned (PT) concrete systems. Fig. 1 shows the cross section of a seven-wire strand made of six outer wires helically coiled around one center king wire. There are two types of posttensioned structures. One type has monostrands coated with grease and/or a plastic sheath to prevent corrosion. The second type has strands embedded in cementitious material (typically grout) to prevent their exposure to the outside environment and resulting corrosion. This paper focuses on grouted tendons, typical of bridge structures. However, exposed strands have been observed in many grouted PT concrete structures [National Cooperative Highway Research Program (NCHRP) 1998; Florida Dept. of Transportation (FDOT) 2001a, b; American Segmental Bridge Institute (ASBI) 2000; Schupack 2004]. An interface between the cementitious grout, the outside air, and the steel strand (denoted as grout-air-steel interface) is formed where the strand protrudes from the grout. When exposed to moisture conditions, the portion of the strand at this interface is particularly vulnerable to corrosion, especially localized corrosion. Localized corrosion can lead to localized reductions in the tension capacity (C_T) of the stressed strands. Probabilistic models to predict the C_T of stressed strands with grout-air-steel interfaces and exposed to corrosive conditions are necessary to assess the long-term performance of PT systems. The tension capacities of unstressed wires, unstressed strands, and stressed strands are denoted in this study as $C_{T,UW}$; $C_{T,US}$; and $C_{T,SS}$, respectively.

Gardoni et al. (2009) developed probabilistic models to predict $C_{T,US}$ as a function of exposure conditions and time. These models do not consider the axial stress conditions experienced by the strands in prestressed concrete bridges. However, based on AASHTO (2007), a typical strand in a highway bridge in service can experience an axial stress of approximately 1,030 N/mm^2 (150 ksi). Proverbio and Longo (2003), Kovač et al. (2007), and Sanchez et al. (2007) reported that the synergistic effect of high stress levels and corrosive media can influence corrosion susceptibility, especially stress corrosion cracking of prestressing strands. Also, Kovač et al. (2007) reported that cold-drawn prestressing steel has a nonuniform microstructure when no axial stress is

[1]Assistant Professor, Dept. of Civil Engineering, Indian Institute of Technology Madras, Chennai 600036, India; and Former Graduate Student, Zachry Dept. of Civil Engineering, Texas A&M Univ., College Station, TX 77843 (corresponding author). E-mail: pillai@iitm.ac.in

[2]J. L. Frank/Marathon Ashland Petroleum LLC Chair in Engineering, Project Management Professor, Zachry Dept. of Civil Engineering, Texas A&M Univ., 3136 TAMU, College Station, TX 77843.

[3]Professor, Acting School Head and Hal Pritchett Chair, Dept. of Civil and Construction Engineering, Oregon State Univ., 220 Owen Hall, Corvallis, OR 97331.

[4]Associate Professor, Dept. of Civil and Environmental Engineering, Univ. of Illinois at Urbana Champaign, 205 N. Mathews Ave., Urbana, IL 61801.

[5]Professor, Zachry Dept. of Civil Engineering, Texas A&M Univ., 3136 TAMU, College Station, TX 77843.

Note. This manuscript was submitted on March 3, 2013; approved on August 30, 2013; published online on September 2, 2013. Discussion period open until October 9, 2014; separate discussions must be submitted for individual papers. This paper is part of the ***Journal of Materials in Civil Engineering***, © ASCE, ISSN 0899-1561/04014044(10)/$25.00.

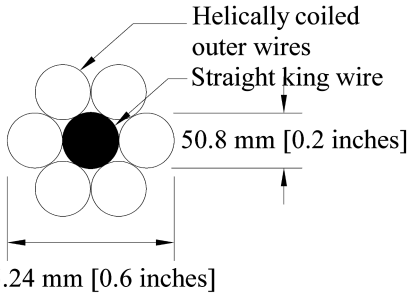

Fig. 1. Cross section of seven-wire strands showing a king wire and six outer wires

present, and transgranular cracks can occur at stress levels of approximately 0.6 times the ultimate strength. In addition, Trejo et al. (2009b) observed that the time-variant loss in $C_{T,SS}$ could be as high as 27% more than the corresponding loss in $C_{T,US}$. These studies indicate that $C_{T,SS}$ could be significantly different from $C_{T,US}$ when exposed to corrosive environments. Therefore, Pillai et al. (2010) developed a probabilistic model to predict $C_{T,SS}$ (denoted as US-SS model). This model was developed using the experimental data from the exposure and the tension testing of unstressed and stressed strands performed by Trejo et al. (2009a). Modification of the US-SS model to suit the exposure conditions, which were not studied by Trejo et al. (2009a), requires additional cumbersome and expensive testing of strands. A less cumbersome and less expensive approach is to predict the stressed-strand capacity, $C_{T,SS}$, as a function of unstressed wire capacity, $C_{T,UW}$. Before discussing this modeling approach, a discussion is provided on why the exposure and tension testing of unstressed and stressed strands is more expensive and cumbersome than the exposure and tension testing of unstressed wires.

Experimental Requirements of Seven-Wire Strand Testing

The exposure and tension testing of unstressed strands requires significant resources associated with the tension testing machine, the strand specimen length, and the laboratory storage space with controlled environment. Similar testing of stressed strands requires additional significant resources associated with the large reaction frames needed to maintain high stress during exposure and significant laboratory storage space to expose the samples.

The requirements for the tension test machine include large capacity and the hydraulic grips sufficient to prevent slippage and stress concentration within the grips. Typically, the ASTM A416 (2006) strands in as-received conditions (i.e., defined as the conditions with negligible corrosion) and with a nominal diameter of 13 or 15 mm (0.5 or 0.6 in.) have a minimum ultimate tensile strength ($MUTS_{strand}$) of approximately 182 kN (41 kips) or 261 kN (58.6 kips), respectively. Tension test machines meeting this capacity requirement are very expensive. The gripping forces and grip lengths are also important to consider for testing. The gripping forces, if applied using a standard V-grip that is manually tightened, are typically not sufficient to resist the large forces during the tension testing of strands. If the stress concentrations within the grips are high, then the strands could fail within or at the edge of the grips. To prevent this and avoid erroneous data collection, long grips [approximately 203 mm (8 in.) long] are needed at both ends of the strand specimen. Therefore, long, powerful, and expensive hydraulic grips are needed.

The total length of strand test specimens is governed by both the gauge length and grip length (i.e., the length of hydraulic grips). For a wire or rectangular plate specimen, the AASHTO T244 (2002), requires that the cross-sectional area at the center region of the specimen be less than that at the end regions, where the specimens are gripped. This reduction in area induces more stress at the center portion, which is defined as the gauge-length region. Because the stress within the gauge-length region is larger than the stress outside the gauge-length region, the specimen will fail within the gauge-length region. However, fabrication of a similar gauge-length region on a seven-wire strand specimen is not possible. This is because the strand specimen consists of seven wires and the mechanisms resisting the tensile stress on a seven-wire strand are complex and different from that of a single wire or plate specimen. The pitch of the helically coiled outer wires has to be taken into account while defining the gauge length of a strand test specimen. Considering these, the AASHTO T 244 (2002) specifically define the gauge length on a strand specimen as the distance between the grips at the ends of the strand specimen and require a minimum gauge length of 610 mm (24 in.). Considering the required gauge length and grip lengths, the total length of a typical strand specimen would be approximately 1,016 mm (40 in.)—the minimum size of the testing region on the test machine. Tension testing machines with this minimum size are very expensive and not available in most structural testing laboratories.

To simulate the typical stress conditions in bridge elements, a high axial stress should be applied to the strands during the entire period of the controlled exposure. Large reaction frames are needed to continuously maintain the high stress on the 1,016-mm (40-in.) long strand specimens. This in turn requires large laboratory space with controlled environments. This is particularly important when exposure conditions are numerous and the strands are to be maintained under constant tensile stress for the entire exposure period. Because of these reasons, the exposure and the tension testing of strands are very cumbersome and expensive.

Experimental Requirements of Wire Testing

Typically, the king wires extracted from ASTM A416 (2006) strands in as-received conditions have a nominal diameter of 4.3 or 5.1 mm (0.17 or 0.20 in.). The C_T of these king wires is typically less than 44.5 kN (10 kips). Therefore, the required machine capacity for performing tension testing of king wires is only a bit more than 44.5 kN (10 kips). Such machines are less expensive compared with the machines required for strand testing. According to AASHTO T244 (2002) and ASTM A370 (1996), the required length of a wire specimen for tension testing is approximately 4 times its nominal diameter. For a king wire specimen, this is 20 mm (0.8 in.). In addition, the standard low-cost V-grips with a grip length of 38 mm (1.5 in.) at each end are adequate for gripping the king wire specimens during tension testing. Considering these, the total required length of a king wire specimen is approximately 58 mm (2.3 in.), which is much smaller than the required length of a strand specimen. Because of the smaller specimen length, the laboratory space required for the exposure of wire specimens is much smaller than that required for strand specimens.

Based on the preceding discussions, the exposure and tension testing of unstressed wire specimens is simpler and less expensive than the exposure and tension testing of unstressed or stressed strands; and therefore, significant economy can be realized if models correlating the capacity of unstressed wires with that of stressed strands can be developed. In other words, a less cumbersome and less expensive approach is to predict the stressed-strand capacity, $C_{T,SS}$, as a function of unstressed wire capacity, $C_{T,UW}$.

This paper first develops the probabilistic models for unstressed wires (denoted as UW models). The primary contributions of this

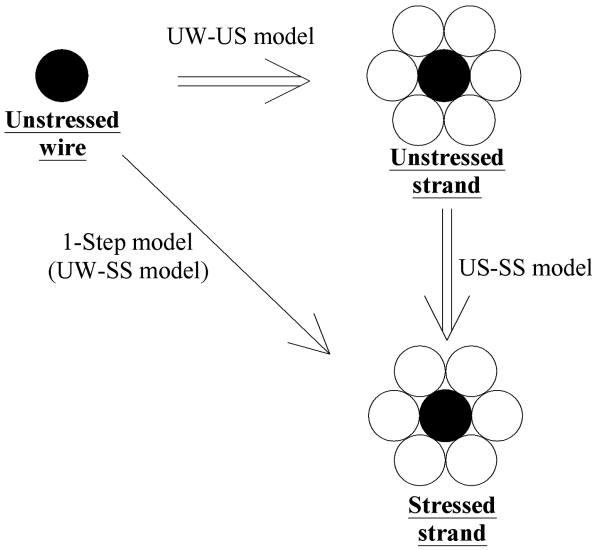

Fig. 2. Graphical representation of the development of the one-step and two-step models

paper are the two probabilistic models (denoted as one-step and two-step models) to predict $C_{T,SS}$ based on the $C_{T,UW}$. Both the one-step and two-step models have their own advantages and disadvantages (discussed later). The one-step model (also known as UW-SS model) to predict $C_{T,SS}$ based on $C_{T,UW}$ is developed by using the experimental data on unstressed wires and stressed strands only (see the single arrow in Fig. 2). The two-step model is developed in two steps as shown by the two double-lined arrows in Fig. 2. In the first step, the UW-US model to predict $C_{T,US}$ from $C_{T,UW}$ is developed, and $C_{T,US}$ is predicted. In the second step, the value of $C_{T,SS}$ is predicted by substituting the median value of $C_{T,US}$ predicted in the first step into the US-SS model. Further details on the development of these models are provided later. These models can be used to determine the $C_{T,SS}$ subjected to grout-air-steel interfaces and various exposure conditions, provided the $C_{T,UW}$ under similar conditions is determined or known.

The remainder of this paper is organized as follows: The significance of this research is presented next; following that, the experimental program and analytical approaches to develop probabilistic tension capacity models are presented; the UW models to determine $C_{T,UW}$ are then presented; and then, the one-step and two-step models to predict $C_{T,SS}$ based on $C_{T,UW}$ are developed. The one-step model captures more uncertainties than each of the two models in the two-step model formulation. Therefore, to ease the presentation, the two-step model is presented before the one-step model. The stress distributions in straight and helical wires in a strand and the tension capacity of wires and strands are then provided; finally, the conclusions drawn are provided.

Research Significance

Probabilistic models to predict $C_{T,SS}$ as a function of time with grout-air-steel interfaces and corrosive exposure conditions are necessary to assess the safety and serviceability of PT concrete systems. The exposure and tension testing of stressed strands are cumbersome and expensive because of the following needs: (1) tension test machines requiring high tension capacity, hydraulic gripping devices with long grip lengths, and long gauge lengths; (2) long test specimens; (3) large reaction frames to maintain high tensile stresses during the entire exposure period; and (4) significant laboratory space with a controlled environment. Based on a 21-month experimental investigation of unstressed and stressed strands and a 12-month experimental investigation of unstressed wires, this paper develops two probabilistic models to predict $C_{T,SS}$ based on $C_{T,UW}$. Future researchers can use these models to determine $C_{T,SS}$, provided the value of $C_{T,UW}$ under similar exposure conditions is known. The value of $C_{T,UW}$ can be determined using an appropriate exposure and tension testing of small king wire specimens, which are shorter and less expensive to test compared with strand specimens.

Experimental Program/Analytical Methods

Experimental Data for Probabilistic Modeling

The experimental program consisted of corrosion exposure and tension testing of unstressed wires, unstressed strands, and stressed strands. These tests were performed under standard room conditions [i.e., defined as 50–70% relative humidity (RH) and 21–29°C (70–85°F)]. Although some variation in corrosion activity will occur from these variations, an assessment using the work by Pour-Ghaz et al. (2009) indicates that corrosion activity from typical temperature variation could be increased by 20%. Because corrosion activity is typically measured on a log scale, a 20% increase is considered insignificant for this study. In addition, Duncan and Ballance (1988) reported that this minimum RH level for corrosion on a metallic surface contaminated by NaCl is 77%. Therefore, the potential variation in corrosion rate owing to this variation in RH is assumed to be negligible in this study, especially when there may be other factors leading to more significant scatter in the corrosion test results. The seven-wire strands [15-mm (0.6-in.) diameter] meeting the ASTM A416 (2006) specifications were used for the unstressed and stressed-strand testing. These strands in as received condition exhibited a mean C_T of 263.7 kN (59.27 kips) with a standard deviation of 1.3 kN (0.29 kips). The minimum ultimate tensile strength of these strands in as-received conditions ($MUTS_{strand}$) was 260.7 kN (58.6 kips). The center king wires [5.1-mm (0.2-in.) diameter] were extracted from seven-wire strands [15-mm (0.6-in.) diameter] and used for the unstressed wire testing. The mean and standard deviation of the C_T of the uncorroded wires were 40.7 kN (9.15 kips) and 0.2 kN (0.05 kips), respectively.

Fig. 3 shows the schematic of a 178-mm (7-in.) long unstressed wire test specimen. The wire pieces were partially embedded in Class A grout [as defined by PTI (2003)] with a water-cementitious ratio of 0.44 to create the grout-air-steel interface (Fig. 3). The fabricated wire specimens were then exposed to cyclic wet-dry exposure (2-week ponding followed by 2-week drying) for exposure times, t, equal to 3, 6, 9, and 12 months (see Table 1). During the 2-week ponding period, the wire specimens were exposed to 0.006, 0.018, and 1.8% sCl^- solutions (% sCl^- is defined as the chloride concentration by mass in the exposure solution). The UW models were developed using the data from the wire testing.

Fig. 4 shows the schematic of a strand test specimen. Each strand specimen was prepared by partially embedding 1,040-mm (41-in.) long strand pieces in cementitious grout to create the grout-air-steel interfaces, similar to the grout-air-steel interfaces in the wire specimens. The materials used and geometry of unstressed and stressed-strand specimens are similar. In the case of the unstressed-strand specimens, no axial stress was applied during the exposure period. In the case of the stressed-strand specimens,

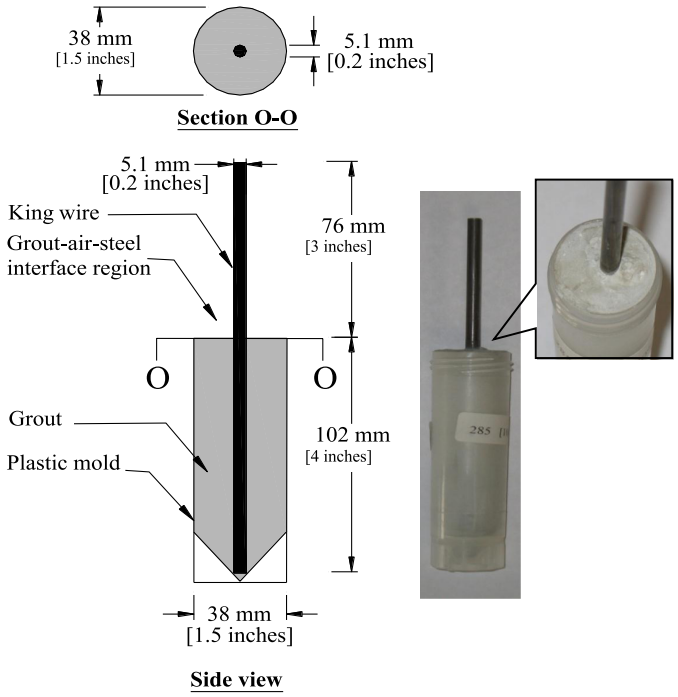

Fig. 3. Schematic and photograph of a wire specimen with grout-air-steel interface

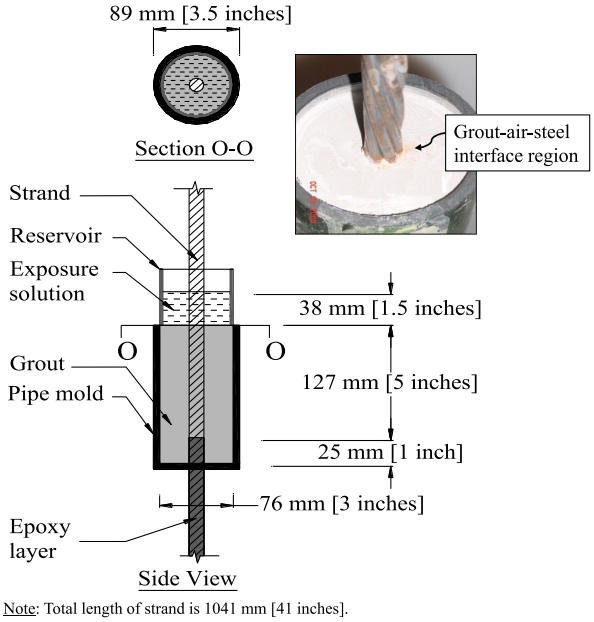

Fig. 4. Schematics of a strand specimen with grout-air-steel interface

an axial tensile stress of approximately 0.56 times the ultimate strength (i.e., 1,030 MPa [150 ksi]) was applied throughout the exposure period. A total of 10 concrete reaction frames, each with six stressed-strand specimens (as shown in Fig. 5), were used for this purpose. The details on the stressing procedures, reaction frames, the gripping mechanisms, and distressing procedures are provided in Trejo et al. (2009a). As shown in Table 1, 60 unstressed-strand specimens were exposed to wet-dry cycles for t equal to 0, 12, and 21 months. This wet-dry exposure regime was similar to the wet-dry exposure regime used in the unstressed wire testing. By using a universal testing machine, the residual $C_{T,US}$ was determined at the end of each t. The UW models and the data from the unstressed-strand testing were then used to develop the UW-US models. As shown in Table 1, 60 stressed-strand specimens were prepared and exposed for t equal to 0, 12, 16, and 21 months; the residual $C_{T,SS}$ was determined at the end of each t. The wet-dry regimes were similar to those used in the testing of unstressed wires. The UW models and the data from the stressed-strand testing were then used to develop the UW-SS models.

Table 1. Number of Wire and Strand Specimens

Wet-dry exposure time, t, (months)	Chloride ion concentration in exposure solution, (% sCl^-)	Specimens with grout-air-steel interface		
		Unstressed wire	Unstressed strand	Stressed strand
3	0.006	3	—	—
	0.018	3	—	—
	1.8	3	—	—
6	0.006	3	—	—
	0.018	3	—	—
	1.8	4	—	—
9	0.006	3	—	—
	0.018	3	—	—
	1.8	4	—	—
12	0.006	3	10	6
	0.018	3	10	6
	1.8	3	10	6
16	0.006	—	—	6
	0.018	—	—	6
	1.8	—	—	6
21	0.006	—	10	8
	0.018	—	10	8
	1.8	—	10	8
Total number of specimens		38	60	60

Note: 10-wire and 24-strand samples were also tested at t equal to 0; (—) indicates no samples were tested.

Probabilistic Modeling of Tension Capacity

Following the general formulation of probabilistic models in Gardoni et al. (2002), $C_{T,UW}$, $C_{T,US}$, and $C_{T,SS}$ can be formulated as follows:

$$R_{C_{T,k}}(\mathbf{x},\boldsymbol{\Theta}_k)=\gamma_k(\mathbf{x},\boldsymbol{\theta}_k)+\sigma_k\varepsilon;\quad k=\text{UW, US, or SS} \tag{1}$$

where $R_{C_{T,k}}(\mathbf{x},\boldsymbol{\Theta}_k)$ = ratio between $C_{T,k}$ and $\text{MUTS}_{\text{strand}}$; $\gamma_k(\mathbf{x},\boldsymbol{\theta}_k)$ = correction function; $\mathbf{x}$ = vector of explanatory functions or regressors; $\boldsymbol{\Theta}_k=(\boldsymbol{\theta}_k,\sigma_k)$ is a vector of unknown model parameters, where $\boldsymbol{\theta}_k=(\theta_{k,1},\ldots,\theta_{k,m})$ is a $1\times m$ vector of model parameters; and $\sigma_k\varepsilon$ = model error, where σ_k = standard deviation of model error and ε = random variable with zero mean and unit standard deviation. In addition to σ_k, the mean absolute percentage error (MAPE) also provides an intuitive measure of model accuracy and is expressed as follows:

$$\text{MAPE}=\frac{1}{n}\sum_{i=1}^{n}\left\{\frac{|\text{Median}[C_{T,k}(\mathbf{x}_i,\boldsymbol{\theta}_k)]-C_{T,k,i}|}{C_{T,k,i}}\right\}\times 100 \tag{2}$$

where n = number of observations; $C_{T,k,i}$ = ith observed value of $C_{T,k}$; and $C_{T,k}$ $(\mathbf{x}_i,\boldsymbol{\theta}_k)$ = predicted value corresponding to $C_{T,k,i}$. Eq. (3) defines the response and explanatory functions that are used in the probabilistic models developed later in this paper as follows:

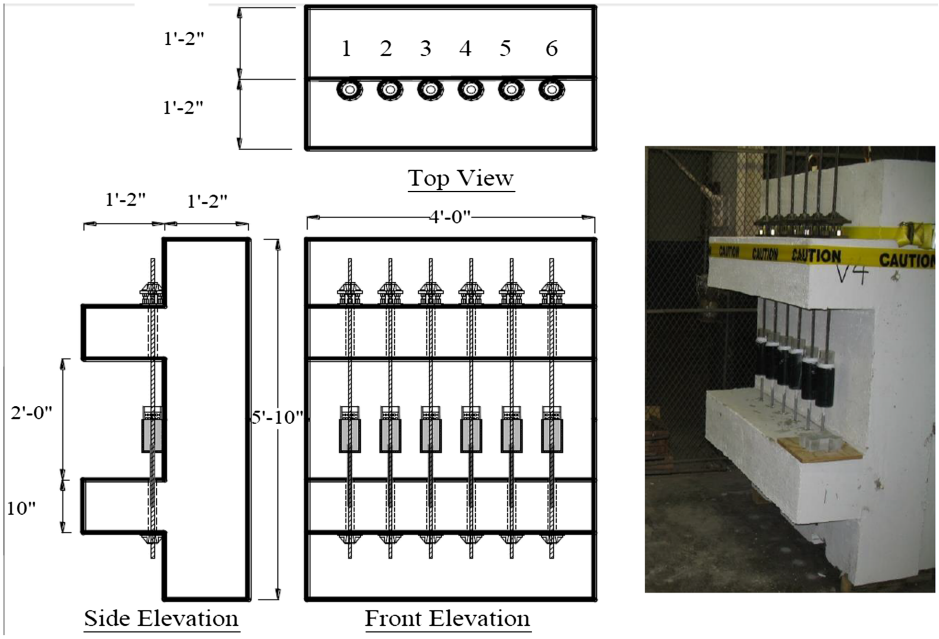

Fig. 5. Concrete reaction frame with six stressed-strand specimens

$$R_{C_{T,\mathrm{UW}}} = \frac{C_{T,\mathrm{UW}}}{\mathrm{MUTS}_{\mathrm{strand}}};\quad R_{C_{T,\mathrm{US}}} = \frac{C_{T,\mathrm{US}}}{\mathrm{MUTS}_{\mathrm{strand}}};\quad R_{C_{T,\mathrm{SS}}} = \frac{C_{T,\mathrm{SS}}}{\mathrm{MUTS}_{\mathrm{strand}}}$$
$$\phi_{\mathrm{wet}} = \frac{\text{Wet-time in a year (months)}}{12};\ 0 \le \phi_{\mathrm{wet}} \le 1\ h_t = \phi_{\mathrm{wet}} \times t(\text{years}) \tag{3}$$

The term h_t can be viewed as a representation of the total wet-time during the entire exposure period, t, in years. The functions (with the exception of h_t) in Eq. (3) are dimensionless. Probabilistic models with dimensionless variables have the following two benefits over those made of variables with specific physical dimensions: (1) the vector, $\boldsymbol{\theta}$, associated with dimensionless variables is also dimensionless; and (2) a dimensionless model is applicable when the values of standardized explanatory functions are within the range of the standardized explanatory functions in the database used to assess the model. Using dimensionless variables typically expands the range of applicability of a probabilistic model. In other words, the models developed in this paper can be used for any seven-wire strands, provided the value of $\mathrm{MUTS}_{\mathrm{strand}}$ is appropriately used. For example, if the models are used to predict the C_T of strands with a nominal diameter of 13 or 15 mm (0.5 or 0.6 in.), then the value of $\mathrm{MUTS}_{\mathrm{strand}}$ should be 182 kN (41 kips) or 261 kN (58.6 kips), respectively. The value of ϕ_{wet} used in these experiments is 0.5. However, a different value can be selected based on the observed wet-dry conditions in the field and Eq. (3).

Probabilistic Capacity Models for Unstressed Wires

The critical chloride threshold level, $\mathrm{Cl}_{\mathrm{threshold}}$, is defined as the minimum amount of chloride concentration required at the steel surface to initiate corrosion. Trejo et al. (2009a) concluded that the $\mathrm{Cl}_{\mathrm{threshold}}$ for the ASTM A416 (2006) steel is greater than 0.06% sCl^-. The rate of corrosion when the percentage of sCl^- is below the $\mathrm{Cl}_{\mathrm{threshold}}$ would be different from that when the percentage of sCl^- is above the $\mathrm{Cl}_{\mathrm{threshold}}$. Therefore, this section formulates and assesses two UW models to predict the $C_{T,\mathrm{UW}}$ when the wires are exposed to solutions with the percentage of sCl^- below and above the $\mathrm{Cl}_{\mathrm{threshold}}$ (denoted as $\mathrm{UW}_{\mathrm{below\ threshold}}$ and $\mathrm{UW}_{\mathrm{above\ threshold}}$ models, respectively).

As a first step in the modeling process, diagnostic plots are developed to study the effect of the percentage of sCl^- and t on $C_{T,\mathrm{UW}}$. Figs. 6(a and b) show that the rate of capacity loss was reduced after 9 months when exposed to 0.006 and 0.018% sCl^- solutions (i.e., less than the $\mathrm{Cl}_{\mathrm{threshold}}$); therefore, $C_{T,\mathrm{UW}}$ is modeled as a power function of h_t for the cases when the percentage of sCl^- is less than the $\mathrm{Cl}_{\mathrm{threshold}}$. This reduction in the rate of loss of $C_{T,\mathrm{UW}}$ is attributed to the presence of less soluble corrosion products around the steel surface, which is typically the case when the chloride exposure level is below the $\mathrm{Cl}_{\mathrm{threshold}}$. The presence of less soluble corrosion products around the steel surface can reduce the oxygen availability to the underlying bare steel resulting in a small corrosion rate. On the other hand, as shown in Fig. 6(c), when the percentage of sCl^- was 1.8% sCl^- (i.e., above the $\mathrm{Cl}_{\mathrm{threshold}}$), the rate of loss of $C_{T,\mathrm{UW}}$ did not change significantly even after 9 months of exposure. This is likely because the solubility of corrosion products is high when the percentage of sCl^- is larger than the $\mathrm{Cl}_{\mathrm{threshold}}$, resulting in similar oxygen availability and similar corrosion rate as a function of time. Therefore, $C_{T,\mathrm{UW}}$ is modeled as a linear function of h_t for the cases when percentage of sCl^- is greater than or equal to the $\mathrm{Cl}_{\mathrm{threshold}}$. The general expression for both the $\mathrm{UW}_{\mathrm{below\ threshold}}$ and $\mathrm{UW}_{\mathrm{above\ threshold}}$ models is as follows:

$$R_{C_{T,\mathrm{UW}}}(\mathbf{x}, \boldsymbol{\Theta}_{\mathrm{UW}}) = \gamma_{\mathrm{UW}}(\mathbf{x}, \boldsymbol{\theta}_{\mathrm{UW}}) + \sigma_{\mathrm{UW}}\varepsilon$$
$$= \theta_{\mathrm{UW},0} + \theta_{\mathrm{UW},1} h_t^{\theta_{\mathrm{UW},2}} + \sigma_{\mathrm{UW}}\varepsilon \tag{4}$$

where the terms are as defined in Eq. (1). The importance sampling technique (Gardoni et al. 2002) is used to assess the model parameters. For the $\mathrm{UW}_{\mathrm{below\ threshold}}$ model (power model), the values of $\theta_{\mathrm{UW},0}$, $\theta_{\mathrm{UW},1}$, $\theta_{\mathrm{UW},2}$, and σ_{UW} are assessed using the data from the wire specimens exposed to 0.006 and 0.018% sCl^-. For the $\mathrm{UW}_{\mathrm{above\ threshold}}$ model (linear model), the value of $\theta_{\mathrm{UW},2}$ is set equal to 1 and the values of $\theta_{\mathrm{UW},0}$, $\theta_{\mathrm{UW},1}$, and σ_{UW} are assessed using the data from the specimens exposed to 1.8% sCl^-. Table 2 shows that the MAPE values of $\mathrm{UW}_{\mathrm{below\ threshold}}$ and $\mathrm{UW}_{\mathrm{above\ threshold}}$ models are 2.8 and 2.6%, respectively. The COVs of the σ_{UW} for these

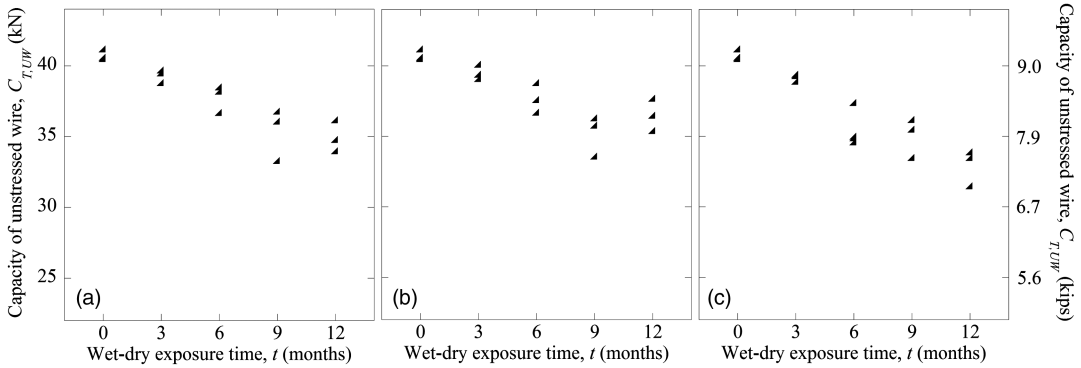

Fig. 6. Scatter plot of unstressed wire capacity, $C_{T,\mathrm{UW}}$, versus exposure time, t: (a) 0.006% sCl^-; (b) 0.018% sCl^-; (c) 1.8% sCl^-

Table 2. MAPE and Posterior Statistics of Probabilistic Models

Model identification	MAPE (%)	Parameter	Mean	Standard deviation	COV	Coefficient of variation	
						$\theta_{k,0}$	$\theta_{k,1}$
$\mathrm{UW}_{\text{below threshold}}$ model for $C_{T,\mathrm{UW}}$	2.8	$\theta_{\mathrm{UW},0}$	0.1565	0.0014	0.01	1	—
		$\theta_{\mathrm{UW},1}$	−0.0026	0.0011	−0.41	−0.59	1
		$\theta_{\mathrm{UW},2}$	0.8289	0.1612	0.19	−0.45	0.98
		σ_{UW}	0.0041	0.0005	0.12	—	—
$\mathrm{UW}_{\text{above threshold}}$ model for $C_{T,\mathrm{UW}}$	2.6	$\theta_{\mathrm{UW},0}$	0.1555	0.0022	0.01	1	—
		$\theta_{\mathrm{UW},1}$	−0.0023	0.0003	−0.13	−0.84	1
		$\theta_{\mathrm{UW},2}$	1.0000	0.0000	0.00	—	—
		σ_{UW}	0.0050	0.0033	0.66	—	—
UW-US model for $C_{T,\mathrm{US}}$	3.3	$\theta_{\mathrm{US},0}$	2.8020	0.1904	0.07	1	—
		$\theta_{\mathrm{US},1}$	0.5399	0.0337	0.06	−0.99	1
		σ_{US}	0.0374	0.0030	0.08	—	—
Two-step model for $C_{T,\mathrm{SS\text{-}2}}$	7.19	$\theta_{\mathrm{SS\text{-}2},0}$	0.9463	0.0064	0.01	1	—
		$\theta_{\mathrm{SS\text{-}2},1}$	2.0301	0.0773	0.04	0.47	1
		$\sigma_{\mathrm{SS\text{-}2}}$	0.0411	0.0034	0.08	—	—
One-step model for $C_{T,\mathrm{SS}}$	6.7	$\theta_{\mathrm{SS},0}$	7.7492	0.9532	0.12	1	—
		$\theta_{\mathrm{SS},1}$	1.0924	0.0617	0.06	0.99	1
		σ_{SS}	0.0619	0.0047	0.08	—	—

Note: k = UW, US, SS-2, or SS.

two models are 0.12 and 0.66, respectively. The small MAPE values suggest that the model can provide a sufficiently accurate prediction.

In this paper, a validation plot is defined as the scatter plot between the observed and predicted values of the C_T of strands. Fig. 7 shows the validation plots for $\mathrm{UW}_{\text{below threshold}}$ and $\mathrm{UW}_{\text{above threshold}}$ models. For a perfect prediction model, the predicted and observed capacities should line up along the 1:1 solid line. However, owing to variations in the actual exposure conditions and the observed values of $C_{T,\mathrm{UW}}$, possible measurement errors and possible model errors resulting from missing variables in Eq. (1) or an inaccurate model form in Eq. (4), there is a scatter around the 1:1 line. In particular, different values of $C_{T,\mathrm{UW}}$ are observed from wire samples with identical combinations of test variables. The two dashed lines in the validation plots delimit the region within one standard deviation from the 1:1 line. In general, the data in Fig. 7 are spread (with an approximately equal width) along the 1:1 line. This indicates an approximate agreement with the homoskedasticity assumption (i.e., similar statistical variance). The homoskedasticity assumption means that the variance of model error is approximately constant and independent of the predictor variables. The normality assumption means that the model error follows a normal distribution. The validity of this assumption is verified using appropriate diagnostic plots (Rao and Toutenburg 1997). The $\mathrm{UW}_{\text{below threshold}}$ and $\mathrm{UW}_{\text{above threshold}}$ models can be used to predict $C_{T,\mathrm{UW}}$ at 12, 16, or 21 months of wet-dry exposure and can then be compared with $C_{T,\mathrm{US}}$ and $C_{T,\mathrm{SS}}$ at 12, 16, or 21 months of wet-dry exposure to develop the two-step and one-step models in the following two sections. However, for a test to be useful, it should ideally be completed in a reasonable time, and these models allow prediction of strand strength using results obtained in 12 months.

Two-Step Probabilistic Capacity Model for Stressed Strands

The two-step model to predict $C_{T,\mathrm{SS}}$ based on $C_{T,\mathrm{UW}}$ is developed in this section. In the first step, the UW-US model to predict $C_{T,\mathrm{US}}$ as a function of $C_{T,\mathrm{UW}}$ is formulated and assessed. In the second step, the value of $C_{T,\mathrm{US}}$ (predicted using the UW-US model) is substituted into the US-SS model developed by Pillai (2009) to form the two-step model.

The UW-US model in the first step is developed using the median of $C_{T,\mathrm{UW}}$ that is predicted using the UW models and the observed values of $C_{T,\mathrm{US}}$. The hollow triangular markers in Fig. 8 show the observed values of $C_{T,\mathrm{US}}$. Within the ellipse in

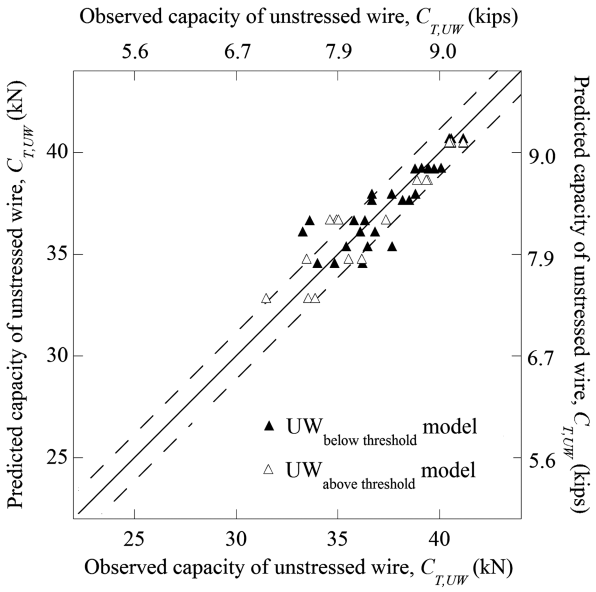

Fig. 7. Validation plots for the UW models to predict $C_{T,\mathrm{UW}}$

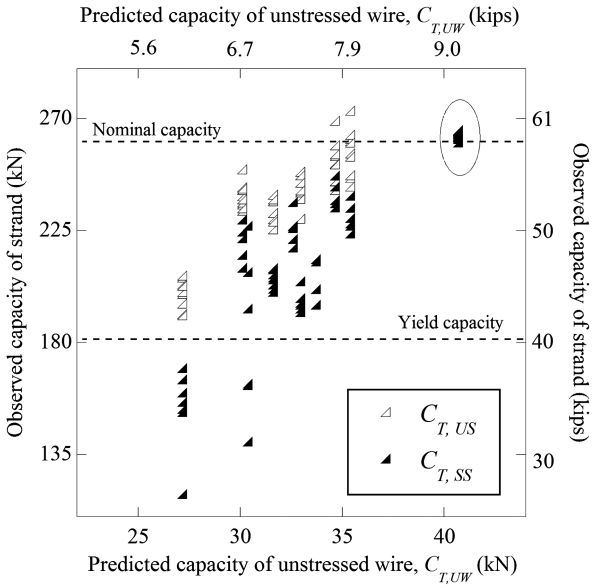

Fig. 8. Scatter plots between the $C_{T,\mathrm{UW}}$, and the $C_{T,\mathrm{US}}$, and $C_{T,\mathrm{SS}}$

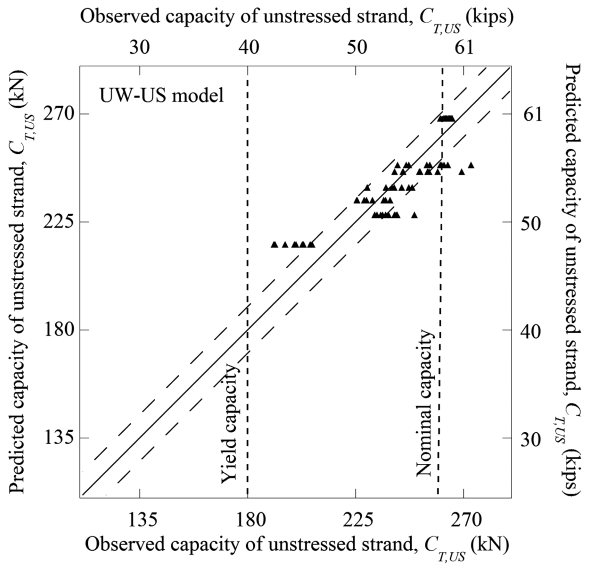

Fig. 9. Validation plots for the unstressed wire unstressed-strand model

the top right corner of this figure, an equal number of hollow markers and solid markers exists, but they are invisible. Preliminary assessment indicated that a power function of $C_{T,\mathrm{UW}}$ is a good approximation and is incorporated into the probabilistic model form as follows:

$$R_{C_{T,\mathrm{US}}}(\mathbf{x},\boldsymbol{\Theta}_{\mathrm{US}}) = \gamma_{\mathrm{US}}(\mathbf{x},\boldsymbol{\theta}_{\mathrm{US}}) + \sigma_{\mathrm{US}}\varepsilon = \theta_{\mathrm{US},0}[\gamma_{\mathrm{UW}}(\mathbf{x},\boldsymbol{\theta}_{\mathrm{UW}})]^{\theta_{\mathrm{US},1}} + \sigma_{\mathrm{US}}\varepsilon \quad (5)$$

where $\gamma_{\mathrm{UW}}(\mathbf{x},\boldsymbol{\theta}_{\mathrm{UW}}) = \theta_{\mathrm{UW},0} + \theta_{\mathrm{UW},1} h_t^{\theta_{\mathrm{UW},2}}$ and other terms are as defined in Eq. (1). This model is assessed using the same procedures that are used to assess the UW models in previous section. Table 2 shows the posterior statistics of the UW-US model. The MAPE of the full model form is 3.3%. Also, the COVs of all the parameter estimates are reasonably small. The value of σ_{US} is also reasonable (i.e., 0.0374). The validation plot in Fig. 9 shows that the UW-US model provides reasonably good estimation of $C_{T,\mathrm{US}}$. Hence, it is concluded that the UW-US model approximately satisfies the homoskedasticity assumption. The UW-US model to predict $C_{T,\mathrm{US}}$ from $C_{T,\mathrm{UW}}$ has now been developed. The nominal cross-sectional area of the seven-wire strand used in the field is approximately seven times the cross-sectional area of a single king wire. For example, the strands and king wires used in this study had nominal cross-sectional areas of 140 and 20.4 mm^2 (0.217 and 0.032 in.^{2}), respectively. Although the UW-US model captures the effects of this increase in area and the flower-like shape of the cross section of the strand on its C_T, it does not capture the effect of the high axial stresses that are experienced by the strands on bridges.

In the second step, to capture the effect of the high axial stress, the two-step model is formulated by nesting the correction function, $\gamma_{\mathrm{US}}(\mathbf{x},\boldsymbol{\theta}_{\mathrm{US}})$, of the UW-US model in Eq. (5) into the US-SS model (Pillai 2009) as follows:

$$\begin{aligned} R_{C_{T,\mathrm{SS}}}(\mathbf{x},\boldsymbol{\Theta}_{\text{SS-2}}) &= \gamma_{\text{SS-2}}(\mathbf{x},\boldsymbol{\theta}_{\text{SS-2}}) + \sigma_{\text{SS-2}}\varepsilon \\ &= \theta_{\text{SS-2},0}\{\gamma_{\mathrm{US}}(\mathbf{x},\boldsymbol{\theta}_{\mathrm{US}})\}^{\theta_{\text{SS-2},1}} + \sigma_{\text{SS-2}}\varepsilon \\ &= \theta_{\text{SS-2},0}\{\theta_{\mathrm{US},0}[\gamma_{\mathrm{UW}}(\mathbf{x},\boldsymbol{\theta}_{\mathrm{UW}})]^{\theta_{\mathrm{US},1}}\}^{\theta_{\text{SS-2},1}} + \sigma_{\text{SS-2}}\varepsilon \end{aligned} \quad (6)$$

where the terms are as defined in Eq. (1); and "2" in the subscript refers to the two-step model. Table 2 summarizes the MAPE and posterior statistics of the two-step model. The MAPE, $\sigma_{\text{SS-2}}$, and the COVs of the model parameters are reasonably small. The hollow triangular markers in Fig. 10 show that the two-step model can provide reasonably good prediction of $C_{T,\mathrm{SS}}$. However, this two-step model has a drawback. In the second step of the two-step model development, the term σ_{US} in the UW-US model [Eq. (5)] is not included in the two-step model. This results in not capturing the uncertainties attributable to the area and flower-like shape of the strand cross section. Therefore, the one-step model that captures the cumulative effects of the area and flower-like shape of the cross section and the axial stress on the C_T of strands is developed next.

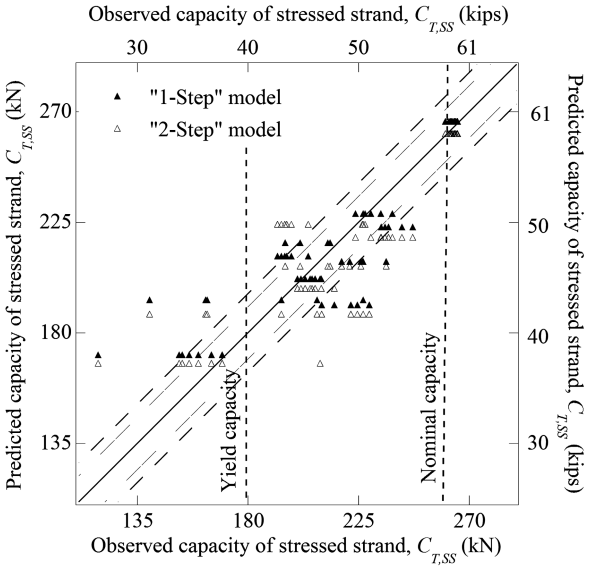

Fig. 10. Validation plots for the one-step and two-step models

One-Step Probabilistic Capacity Model for Stressed Strands

This section presents the development of the one-step model using the median predicted values of $C_{T,\mathrm{UW}}$ and the observed data on $C_{T,\mathrm{SS}}$. The solid triangular markers in Fig. 8 show the scatter plot between $C_{T,\mathrm{UW}}$ and $C_{T,\mathrm{SS}}$. Each $C_{T,\mathrm{UW}}$ value is predicted using the UW models. A preliminary analysis of these data indicated that $C_{T,\mathrm{SS}}$ can be expressed as a power function of $C_{T,\mathrm{UW}}$. Following Eq. (1), the probabilistic model for $C_{T,\mathrm{SS}}$ is formulated as follows:

$$R_{C_{T,\mathrm{SS}}}(\mathbf{x}, \boldsymbol{\Theta}_{\mathrm{SS}}) = \gamma(\mathbf{x}, \boldsymbol{\theta}_{\mathrm{SS}}) + \sigma_{\mathrm{SS}}\varepsilon = \theta_{\mathrm{SS},0}[\gamma(\mathbf{x}, \boldsymbol{\theta}_{\mathrm{UW}})]^{\theta_{\mathrm{SS},1}} + \sigma_{\mathrm{SS}}\varepsilon \quad (7)$$

where $\gamma(\mathbf{x}, \boldsymbol{\theta}_{\mathrm{UW}}) = \theta_{\mathrm{UW},0} + \theta_{\mathrm{UW},1} h_t^{\theta_{\mathrm{UW},2}}$ and the other terms are as defined in Eq. (1). The multiplicative parameter, $\theta_{\mathrm{SS},0}$, supports that $C_{T,\mathrm{SS}}$ should be zero when $C_{T,\mathrm{UW}}$ reaches zero. This model has a similar form as the UW-US model and is assessed using the same procedures that are used to assess the UW and UW-US models. Table 2 summarizes the MAPE and posterior statistics of the one-step model. The MAPE, σ_{SS}, and the COVs of the model parameters are reasonably small, considering the scatter in the observed data from the samples with similar exposure conditions. The solid triangular markers in Fig. 10 show a comparison between predicted and observed values of $C_{T,\mathrm{SS}}$ at t equal to 0, 12, 16, and 21 months. Approximately 85% of the data points fall along the 1:1 line and within $\pm\sigma$ region. This shows a reasonably good model prediction and agreement to the normality and homoskedasticity assumptions. Considering the inherent scatter in the corrosion phenomenon, the model exhibits no serious systematic bias or residual trend, except when $C_{T,\mathrm{SS}}$ is below yield strength.

Both the two-step and one-step models show similar predictions. The $\pm\sigma$ region of the two-step model (inclined, long-dash lines in Fig. 10) is narrower than that of the one-step model (inclined, short-dash lines in Fig. 10). However, the MAPE of the one-step model (i.e., 6.73%) is slightly less than that of the two-step model (i.e., 7.19%). Moreover, the one-step model provides better prediction near the $\mathrm{MUTS}_{\mathrm{strand}}$ region than that predicted by the two-step model. In addition, the two-step model does not capture the uncertainties attributable to the area and flower-like shape of the strand cross section; the one-step model captures the cumulative effects of the cross-sectional area and shape and the stress. For these reasons, the one-step model should be preferred over the two-step model for predicting $C_{T,\mathrm{SS}}$.

Discussion on the Tension Capacities of Wires and Strands

The C_T of a solid wire is directly proportional to its cross-sectional area. According to AASHTO T244 (2002), a seven-wire strand is defined to have failed when one or more wires break. Therefore, the C_T of a seven-wire strand is not directly proportional to its total cross-sectional area and depends on the applied load and available cross-sectional areas of individual wires. Also, depending on the applied load and available cross-sectional areas on each wire, if one wire failed, the redistribution of load would result in subsequent failure of other wires in the same strand. This section first discusses the stress distribution (during the tension testing) among the seven wires in an as-received strand and a corroded strand. Then, the relationship between $C_{T,\mathrm{UW}}$ and $C_{T,\mathrm{US}}$ and between $C_{T,\mathrm{UW}}$ and $C_{T,\mathrm{SS}}$ is discussed.

Stress Distribution in an As-Received Strand and a Corroded Strand

As mentioned earlier, the mean C_T of as-received wires and strands are 40.7 kN (9.15 kips) and 263.7 kN (59.27 kips), respectively, resulting in a strand-to-wire capacity ratio of 6.48 ($59.27/9.15 = 6.48$). Therefore, the C_T of a seven-wire strand could be approximately 6.48 times the C_T of a straight wire (rather than seven times the C_T of a straight wire). This is because the maximum stresses (during the tension testing) experienced by all the wires in an as-received strand are unequal; and the king wire experiences more stress than the helical wires and breaks before the helical wires break. On the other hand, during the tension testing of a corroded strand, a helical wire may break before the king wire if the helical wires are more corroded than the king wire.

The stress-strain curves for individual wires in a strand (obtained from a single strand test and not from multiple tests on king wire and outer wires) could not be found in the literature and were not obtained through this research as well. However, the conceptual elongation-stress curves for king and helical wires during the tension testing of an as-received and a corroded strand, respectively, are shown in Fig. 11. In Fig. 11, the abscissa and ordinate indicate the elongation along the straight axis of the strand and the stress along the straight axis (for king wire) and along the helical path (for helical wires). The solid and dashed curves indicate the king and helical wires, respectively; K_{yield} and H_{yield} indicate the approximate yield points of the king and helical wires, respectively; K_{end} and H_{end} indicate the point at which the tension test ends. In Fig. 11(a), the dotted line beyond H_{end} until H′ corresponds to the unutilized elongation and stress capacities of helical wires in the as-received strand. In Fig. 11(b), the dotted line beyond K_{end} (i.e., until K') corresponds to the unutilized elongation and stress capacities of the king wire in a corroded strand. The king wire is oriented along the straight axis of the strand, whereas the helical wires are oriented at an angle ϕ_0 (i.e., the helix angle measured with reference to the axis of the strand). As the total applied tensile force on the strand increases, both the king wire and the helical wires in a strand stretch; but the helical wires unwind, resulting in a reduction in the helix angle of wires, so $\phi < \phi_0$. In both Figs. 11(a and b), the portion O-H_{unwind} of the curves indicate the unwinding of helical wires.

In an as-received strand, from the strain compatibility along the axis of the strand, the strain in the king wire (along the straight axis)

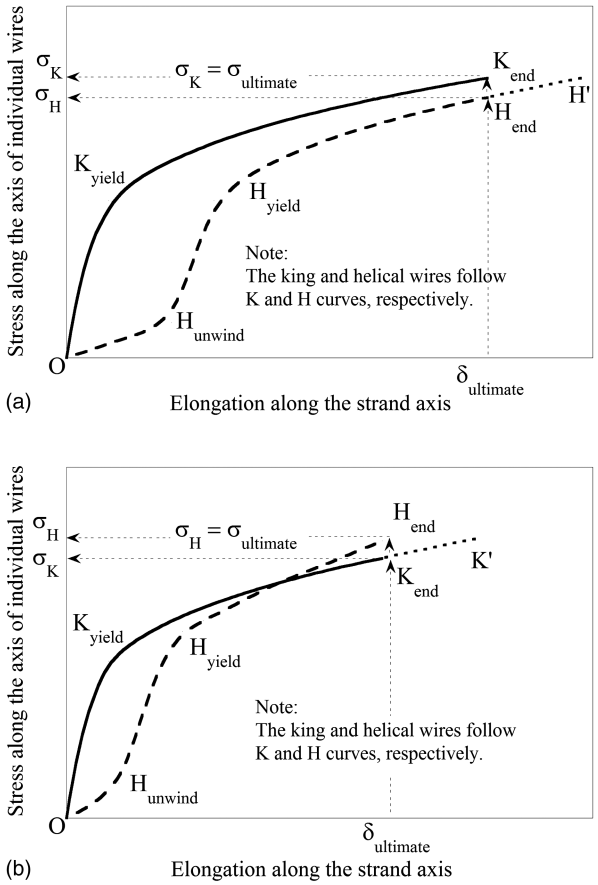

Fig. 11. Conceptual relationship between stress and axial elongation of king and helical wires in a strand: (a) as-received strand; (b) corroded strand

is more than the strains on the helical wires (along their helical axes). Therefore, the king wire experiences more stress than each individual helical wire and breaks when the axial elongation on all the wires reach δ_{ultimate} [Fig. 11(a)]. At this stage, the stress on the helical wire, σ_H, is less than σ_{ultimate}. Therefore, it can be concluded that the king wire breaks before any helical wires break, as was observed in the testing program for as-received strand specimens.

In the case of a corroded strand [Fig. 11(b)], the stress distribution depends on the residual cross-sectional area at the weakest location of the corroded individual wires. Note that the strand portion within the grips might not have corroded. Also, the frictional forces between the corroded strands can play a role in their tension resisting mechanism (MacDougall and Bartlett 2003). The localized corrosion and friction between the wires can result in a complex stress distribution among the seven wires in corroded strands. The details of this complex corrosion and capacity behavior were not investigated in this research. In the laboratory tension testing of corroded strands, the stress on individual helical wire (i.e., σ_H) depends on the localized corrosion and the resulting residual cross-sectional areas of individual wires, especially at the weakest portion of the weakest wire. This indicates that at least one helical wire can experience the stress equal to its stress capacity, σ_{ultimate}, and break when the elongation (along the strand axis) on all the wires reached δ_{ultimate}. At this stage, the stress on the king wire, σ_K, was less than σ_{ultimate}. Therefore, at least one helical wire can break before the king wire breaks in a corroded strand. In short, the C_T of a strand is not directly proportional to the total cross-sectional area; it depends on the cross-sectional areas of individual wires, which in turn are influenced by the corrosion rate of individual wires.

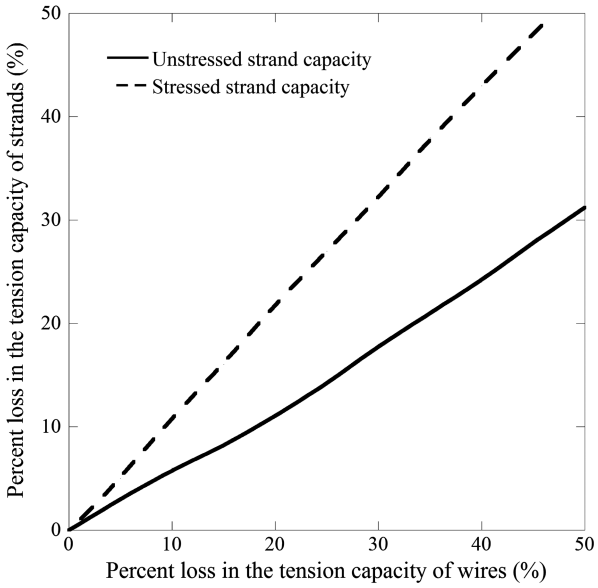

Fig. 12. Comparison between the reduction in CT of wires and strands

Tension Capacities of Wires and Strands

The solid line in Fig. 12 shows the relationship between $C_{T,\text{UW}}$ and $C_{T,\text{US}}$. Although there are chances of severe corrosion attributable to the flower-like shape and sharp angles of a strand cross section, the slope of the solid line is less than unity. This indicates that the rate of loss of $C_{T,\text{US}}$ is less than the rate of loss of the C_T of a hypothetical, unstressed solid wire with nominal cross-sectional area equal to that of an unstressed strand. This is likely a result of the complex stress distribution and corrosion mechanisms (as discussed earlier) in an unstressed strand as compared with those in an unstressed solid wire.

The dashed line in Fig. 12 shows the relationship between $C_{T,\text{UW}}$ and $C_{T,\text{SS}}$ and is steeper than the solid line. This indicates that the rate of reduction in $C_{T,\text{SS}}$ is larger than that of $C_{T,\text{US}}$. This substantiates the earlier findings by Proverbio and Longo (2003), Kovač et al. (2007), Sanchez et al. (2007), and Trejo et al. (2009b) that the high axial stress has significant influence in the corrosion and resulting loss in C_T. In other words, the synergistic effects of high axial stress (i.e., prestress forces) and high chloride exposure levels can cause more adverse effects than the favorable effects attributed to the mechanical protection offered by the outer wires and the possibly dense corrosion products in the interstitial spaces between the seven wires. Considering the fact that strands in PT structures experience very high axial stress, the one-step model should be used to predict the tension capacity of strands in highway bridges.

Summary and Conclusions

A 21-month-long unstressed wire, unstressed strand, and stressed strand corrosion test program (with 38, 60, and 60 specimens, respectively) was conducted. Based on the data from unstressed wire testing, unstressed wire models were developed to predict the tension capacity of wire specimens with grout-air-steel interface and exposed to chloride conditions below and above the critical chloride threshold of the prestressing steel meeting ASTM A416 (2006) specifications. The predicted capacities of unstressed wires, the experimental data from 60 unstressed-strand specimens and an existing model by Pillai (2009) were used to develop two-step model to predict the tension capacity of stressed strands. This

two-step model has the following three merits: (1) It is possible to learn about the behavior of unstressed strands based on the unstressed wire behavior; (2) more is learned about the behavior of stressed strand by breaking down the differences in the behavior between stressed strand and unstressed wires into the contribution that results from considering a strand instead of a wire when they are both unstressed and owing to adding a tension force (i.e., going from unstressed strands to stressed strands); and (3) if data are available on unstressed strands, the second model in the two-step formulation can be used to compute the response of stressed strands. Therefore, in the future, testing can be done on unstressed strands and then the response of stressed strands can be computed using the second model in the two-step formulation. However, the two-step model has a demerit of not being able to explicitly capture the uncertainty attributed to the area and flower-like shape of the strand cross section. Therefore, the predicted capacities of unstressed wires and the experimental data from 60 stressed-strand specimens were used to develop the one-step model to predict the tension capacity of stressed strands. The one-step model captures the cumulative uncertainty attributable to the area, shape of the strand cross section, and the applied stress. The developed models can be used to predict the tension capacity of strands subjected to various exposure conditions, provided the tension capacity of unstressed wires subjected to similar exposure conditions and the minimum ultimate tensile strength of strands ($MUTS_{strand}$) are known. It was also found that the tension capacity of a strand is not directly proportional to the total cross-sectional area; it depends on the cross-sectional areas of individual wires, which in turn is influenced by the corrosion rates of individual wires. The differences in the stress-strain behavior of individual wires in strands with varying degrees of corrosion deserve investigation.

Acknowledgments

This research was performed at Texas Transportation Institute and Zachry Department of Civil Engineering, Texas A&M University, College Station, Texas, through the sponsored project No. 0-4588 (2003-2008) from the Texas Department of Transportation (TxDOT), Austin, Texas. The authors also acknowledge the assistance from Mr. Jeff Perry, Mr. Matt Potter, Mr. Scott Crauneur, Mr. Scott Dobrovolny, Mr. Robert Kocman, Mr. Ramesh Kumar, and Prof. Daren Cline.

References

AASHTO T244. (2002). "Standard method of test for mechanical testing of steel products." Washington, DC.

AASHTO. (2007). "AASHTO LRFD bridge design specifications." Washington, DC.

American Segmental Bridge Institute (ASBI). (2000). "American segmental bridge institute grouting committee, interim statement on grouting practices." Phoenix, AZ.

ASTM A370. (1996). "Standard test methods and definitions for mechanical testing of steel products." West Conshohocken, PA.

ASTM A416. (2006). "Standard specification for steel strand, uncoated seven-wire for prestressed concrete." West Conshohocken, PA.

Duncan, J. R., and Ballance, J. A. (1988). "Marine salts contribution to atmospheric corrosion." *Degradation of metals in the Atmosphere, ASTM STP 965*, S. W. Dean and T. S. Lee, eds., ASTM, West Conshohocken, PA, 317–326.

Florida Dept. of Transportation (FDOT). (2001a). "Mid-bay bridge post-tensioning evaluation—Final report." Corven Engineering, Tallahassee, FL.

Florida Dept. of Transportation (FDOT). (2001b). "Sunshine skyway bridge post-tensioned tendons investigation." Parsons Brinckerhoff Quade and Douglas, Tallahasse, FL.

Gardoni, P., Pillai, R. G., Trejo, D., Hueste, M. D., and Reinschmidt, K. (2009). "Probabilistic capacity models for corroding posttensioning strands calibrated using laboratory results." *J. Eng. Mech.*, 10.1061/(ASCE)EM.1943-7889.0000021, 906–916.

Gardoni, P. G., Der Kiureghian, A., Mosalam, K. M. (2002). "Probabilistic capacity models and fragility estimates for reinforced concrete columns based on experimental observations." *J. Eng. Mech.*, 10.1061/(ASCE)0733-9399(2002)128:10(1024), 1024–1038.

Kovač, J., Leban, M., and Legat, A. (2007). "Detection of SCC on prestressing steel wire by the simultaneous use of electrochemical noise and acoustic emission measurements." *Electrochemica Acta*, 52(27), 7607–7616.

MacDougall, C., and Bartlett, F. M. (2003). "Tests of unbonded seven-wire tendon with broken outer wires." *ACI Mater. J.*, 100(5), 581–588.

National Cooperative Highway Research Program (NCHRP). (1998). "Durability of precast segmental bridges." *NCHRP Web Document No. 15, Project 20-7/Task 92*, R. W. Poston and J. P. Wouters, Transportation Research Board, National Research Council, Washington, DC.

Pillai, R. G. (2009). "Electrochemical characterization and time-variant structural reliability assessment of post-tensioned, segmental concrete bridges." Ph.D. dissertation, Zachry Dept. of Civil Engineering, Texas A&M Univ., College Station, TX.

Pillai, R. G., Gardoni, P., Trejo, D., Hueste, M. D., and Reinschmidt, K. (2010). "Probabilistic models for the tensile strength of corroding strands in posttensioned, segmental concrete bridges." *J. Mater. Civ. Eng.*, 10.1061/(ASCE)MT.1943-5533.0000096, 967–977.

Post-Tensioning Institute (PTI). (2003). "Specification for grouting of post-tensioned structures." Phoenix, AZ.

Pour-Ghaz, M., Burkan Isgor, O., and Ghods, P. (2009). "The effect of temperature on the corrosion of steel in concrete. Part I: Simulated polarization resistance tests and model development." *Corrosion Sci.*, 51(2), 415–425.

Proverbio, E., and Longo, P. (2003). "Failure mechanisms of high strength steels in bicarbonate solutions under anodic polarization." *Corrosion Sci.*, 45(9), 2017–2030.

Rao, C. R., and Toutenburg, H. (1997). *Linear models, least squares and alternatives*, Springer, New York.

Sanchez, J., Fullea, J., Andrade, C., and Alonso, C. (2007). "Stress corrosion cracking mechanism of prestressing steels in bicarbonate solutions." *Corrosion Sci.*, 49(11), 4069–4080.

Schupack, M. (2004). "PT Grout: Bleedwater voids." *Concr. Int.*, 26(8), 69–77.

Trejo, D., et al. (2009a). "Effects of voids in grouted, post-tensioned, concrete bridge construction." *Rep. No. 0-4588-1*, Texas Transportation Institute, Texas Dept. of Transportation, Austin, TX, ⟨http://tti.tamu.edu/documents/0-4588-1-Vol1.pdf⟩ (Mar. 15, 2014).

Trejo, D., Pillai, R. G., Hueste, M. D., Reinschmidt, K., and Gardoni, P. (2009b). "Parameters influencing corrosion and tension capacity of post-tensioning strands." *ACI Mater. J.*, 106(2), 144–153.